Polymer 100 (2016) 227–237

Contents lists available at ScienceDirect

Polymer

journal homepage: www.elsevier.com/locate/polymer

Synthesis, characterization and dielectric relaxation study of hyperbranched polymers with different molecular architecture

Juan M. Giussi [a, *], Omar Azzaroni [a], Stella Hensel-Bielowka [b], Zaneta Wojnarowska [c, d], Justyna Knapik [c, d], Marian Paluch [c, d]

[a] Instituto de Investigaciones Fisicoquímicas Teóricas y Aplicadas (INIFTA), CONICET-UNLP, CC16, Suc. 4, La Plata, Buenos Aires, Argentina
[b] Institute of Chemistry, University of Silesia, Szkolna 9, 40-006 Katowice, Poland
[c] Institute of Physics, University of Silesia, Uniwersytecka 4, 40-007 Katowice, Poland
[d] Silesian Center for Education and Interdisciplinary Research, 75 Pulku Piechoty 1A, 41-500 Chorzow, Poland

ARTICLE INFO

Article history:
Received 11 May 2016
Received in revised form
1 August 2016
Accepted 7 August 2016
Available online 9 August 2016

Keywords:
Synthetic hyperbranched polymers
Spectroscopic characterization
Thermal and dielectric properties

ABSTRACT

Hyperbranched polymers are macromolecular systems of high branching density. They play a key role in the forefront of macromolecular synthesis for having features different from those of non-hyperbranched polymers and unique properties that make them amenable for use in a variety of applications. This paper presents the results from the synthesis of hyperbranched polymers of different molecular architecture, i.e., spherical and cylindrical. Also characterization of their thermal and dynamic properties is provided. Atom transfer radical polymerization from star and linear pre-former macroinitiators produced hyperbranched systems based on methyl methacrylate and lauryl methacrylate. Thermal characterizations by TGA and DSC allowed different types of interactions and degradation mechanisms as a function of the determined polymer architecture. NMR studies revealed the effect of molecular architecture on monomers tacticity along the molecular brushes. Spherical architecture yielded a higher isotactic percentage than cylindrical architecture did, thus indicating a specific stereochemistry as a function of the macroinitiator morphology. Broadband dielectric spectroscopy, one of the most powerful techniques to study the dynamics of molecular systems revealed not only different patterns of behavior of hyperbranched polymers of different architectures but also results in agreement with NMR on stereochemistry as a function of molecular architecture.

1. Introduction

Hyperbranched polymers are highly branched macromolecules with three-dimensional structures that have received considerable scientific attention in the last decade. One of the most relevant properties of these materials is their high branching density. Consequently, their applicability can be significantly enhanced beyond that of linear polymers [1,2]. These complex architectures have been used in different fields of biomedicine, such as drug delivery, gene delivery, tissue engineering, and diagnosis [3,4]. In many other areas including phase transfer [5], nanotechnology [6,7], solar cells [8] or advanced optical devices [9], the use of hyperbranched polymers is being actively pursued.

These compounds have been widely studied due to the various morphologies that hyperbranched polymers have. Especially attractive is the fact that their unique architecture is related to distinctive physical/chemical properties. The advance in polymer synthesis has led to an enhanced capability to build more complex polymeric architectures, such as gradient polymers [10], polymer brushes [11], graft polymers [12], dendrimers [13], and star polymers [14].

Atom transfer radical polymerization (ATRP) allows one to synthesize hyperbranched polymers of variable molecular architecture [2,15]. ATRP, as well as other mechanisms of control radical polymerization, offers the opportunity to synthesize macromolecules with predetermined molecular weight, low polydispersity, controlled compositions, functionalities, and chain topologies.

Lutz et al. [16] explained the little success of ATRP in attaining control regarding sequence distribution of monomers and tacticity. However, a significant control over tacticity has been reported using specific monomers, monomers with either extremely bulky substituents [17] or a chiral auxiliary [18].

* Corresponding author.
E-mail address: jmgiussi@inifta.unlp.edu.ar (J.M. Giussi).

http://dx.doi.org/10.1016/j.polymer.2016.08.027
0032-3861/

Moreover, to be able to utilize these newly-obtained materials not only are structural studies needed but also an understanding of their dynamics. One of the most powerful techniques to study molecular system dynamics is broadband dielectric spectroscopy. For many years, this method has been successfully applied in the study of polymers [19], especially those of complex molecular architectures [20–22]. Dielectric studies have shown that the complex structures of these compounds are reflected by a multitude of relaxation processes that can be observed above and below the glass transition temperature depending on the mobility of the different parts of the studied systems [23–25].

Since the morphology and nature of the molecular brushes determine the properties and applicability of new materials, the aim of this work is to obtain hyperbranched polymers of tunable morphology, architecture and sequence microstructure of molecular brushes. NMR studies allowed us to analyze the morphologic effect in the stereochemistry of these materials. In addition, thermal and dielectric properties were assessed to investigate the way in which the morphology influenced the dynamics of this interesting group of compounds.

2. Experimental

2.1. Materials

Hyperbranchedbis-MPA polyester-64-hydroxyl, generation 4 (97%, Aldrich), 4-(dimethylamino) pyridine (99%, Aldrich), triethylamine (99%, Sintogran), tetrahydrofuran (RPE, Carlo Erba), 2-bromoisobutyric acid bromide (98%, Aldrich), methanol (RPE, Anedra), chloroform (RPE, Carlo Erba), dimethylsulfoxide (RA, Anedra), CuBr (99,995%, Aldrich), 2,2′-bipyridine (98%, Biopack), poly (2-hidroxyethyl methacrylate) (Mv 300.000, Aldrich), poly methylmethacrylate (Mw 64,020, Aldrich) with stereoregular composition estimated by H NMR of 4,3% isotactic, 39% atactic, and 56,7% syndiotactic. Monomers, methyl methacrylate (99%, Aldrich) and lauryl methacrylate (96%, Aldrich) were freed from the inhibitor by washing with aqueous NaOH solution (10 wt %) and then with water until neutral, dried over anhydrous sodium sulfate, and distilled under reduced pressure before use. The monomer purity was verified by H NMR.

2.2. Hyperbranched polymers synthesis

Scheme 1a illustrates the chemical structure of hyperbranchedbis-MPA polyester-64-hydroxyl, generation 4 (HBP–OH); and Scheme 1b the synthesis procedure of Spherical (MMA-HBPM) and Cylindrical (MMA-PBIEM and LMA-PBIEM) hyperbranched polymers.

2.2.1. Spherical hyperbranched polymers synthesis

Spherical Macroinitiator synthesis [26].The spherical macro initiator (HBPM) was prepared as follows: A solution of 0.78 g (corresponding to 7 mmol of hydroxyl groups) of Hyperbranched *bis*-MPA polyester-64-hydroxyl, generation 4 (ALH-64-OH) in 20 ml of dry THF was added to a solution of 4-(dimethylamino) pyridine (0.97 g, 7.9 mmol) and triethylamine (0.70 g, 0.97 ml, 6.98 mmol) in 7 ml of dry THF under nitrogen atmosphere. Then, 4.80 g (2.58 ml, 20.9 mmol) of 2-bromoisobutyric acid bromide was added dropwise at room temperature. After 48 h, 4-(dimethylamino) pyridine hydrochloride precipitated was filtered off and the solvent containing the macroinitiator was evaporated to half volume. The residual solution was precipitated into methanol. The precipitate was dried under vacuum. Yield was 68%. H NMR (300 MHz, Chloroform-d_1): δ: 1.25–1.40 ppm (–CH_3, 82 H); 1.95 ppm (–C(Br)–$(CH_3)_2$, 176H); 4.20–4.50 (CH_2–OCO, 112 H). M_n = 2050 g/mol, and PDI = 4.4 (SEC chromatogram in Supporting Information).

MMA-HBPM. *ATRP Procedure:* 15 ml of DMSO was placed in a Schlenk flask with magnetic stir and purged with N_2 bubbling for 15 min. Afterwards, 33 mg (0.22 mmol) CuBr and 69 mg (0.44 mmol) Bipy were added (brown coloration was observed due to the metal-ligand complex). After 10 min with nitrogen bubbling, a solution of 1 g (0.22 mmol) HBPM was incorporated in 3 ml of DMSO, and then purged with N_2 bubbling again. The mixture was heated to 60 °C, and polymerization was initiated by adding 2.2 g (22 mmol) of MMA. After 4 h of reaction, the reaction mixture was cooled and the catalyst complex was removed by suction filtration of the reaction mixture through a layer of neutral alumina. The resulting polymer solution was partially evaporated and finally precipitated into methanol. Crude polymer was purified by dissolution in chloroform and re-precipitation into methanol. Yield: 27% with respect to monomer. H NMR (300 MHz, Chloroform-d_1): δ: 0.80–1.10 (–CH_3, 195H); 1.22–1.40 ppm (–CH_3, 108 H); 1.95 ppm (–C(Br)–$(CH_3)_2$, 165H); 3.64 ppm (O–CH_3, 191H); 4.10–4.50 (CH_2–OCO, 112 H). Mn = 11,600 g/mol, PDI = 3.02 (SEC chromatogram in Supporting Information).

2.2.2. Cylindrical hyperbranched polymers synthesis

Cylindrical Macroinitiator Synthesis [27].The macro initiator poly (2-(2-bromoisobutyloxyethyl methacrylate) (PBIEM) was prepared by dissolving 4 g of poly (HEMA) (0.0311 mol OH groups) in 50 ml of anhydrous pyridine. Then 14.3 g α-bromoisobutyryl bromide was added slowly at 0 °C under dry nitrogen. The solution was kept stirring at 0 °C for 2 h and for another 24 h at room temperature. The precipitated pyridinium salt was filtered off, and the solvent was removed by means of a rotary evaporator. The crude product was purified by dissolving in toluene and passing through an Al_2O_3 column, followed by precipitation in methanol. Yield: 78%. H NMR (300 MHz, Chloroform-d_1): δ: 0.99 ppm (-CH_3, 3H); 1.13 ppm (–CH_2–C, 2H); 2.01 ppm (–C(Br)–$(CH_3)_2$, 6H); 4.25 ppm (CH_2–OCOC, 2H); 4.41 ppm (CH_2–OCOCBr, 2H). M_n = 25,700 g/mol, and PDI = 5.6 (SEC chromatogram in Supporting Information).

MMA-PBIEM. *ATRP Procedure:* 25 ml of DMSO was placed in a Schlenk flask with magnetic stir and purged with N_2 bubbling for 15 min. Afterwards, 100 mg (0.35 mmol) of PBIEM was incorporated, and, after 15 min with nitrogen bubbling, 52 mg (0.35 mmol) of CuBr and 110 mg (0.70 mmol) of Bipy were added. After 15 min with nitrogen bubbling, the mixture was heated to 60 °C, bubbling was changed to a constant stream of N_2, and polymerization was initiated by adding 3.5 g (35 mmol) of methyl methacrylate monomer. After 4 h, the reaction mixture was cooled and precipitated into methanol. Crude polymer was purified by dissolution in chloroform, suction filtration through a layer of neutral alumina and re-precipitation into methanol. Yield: 62% with respect to monomer. H NMR (300 MHz, Chloroform-d_1): δ: 0.80–1.27 ppm (–CH_3, 3H); 1.70–2.10 ppm (–CH_2–C, 2H); 3.45–3.80 ppm–OCH_3, 3H). M_n = 500,400 g/mol, and PDI = 5.4 (SEC chromatogram in Supporting Information).

LMA-PBIEM. *ATRP Procedure:* 25 ml of THF was placed in a Schlenk flask with magnetic stir and purged with N_2 bubbling for 15 min. Later on, 100 mg (0.35 mmol) of PBIEM was incorporated, and, after 15 min with nitrogen bubbling, 52 mg (0.35 mmol) of CuBr and 110 mg (0.70 mmol) of Bipy were added. After 15 min with nitrogen bubbling, the mixture was heated to 60 °C, nitrogen bubbling was removed, and the polymerization was initiated by adding 8.9 g (35 mmol) of lauryl methacrylate monomer. After 28 h, the reaction mixture was cooled and precipitated into isopropanol. Crude polymer was purified by dissolution in chloroform, suction filtration through a layer of neutral alumina and re-precipitation into isopropanol. Yield: 35% with respect to monomer. H NMR

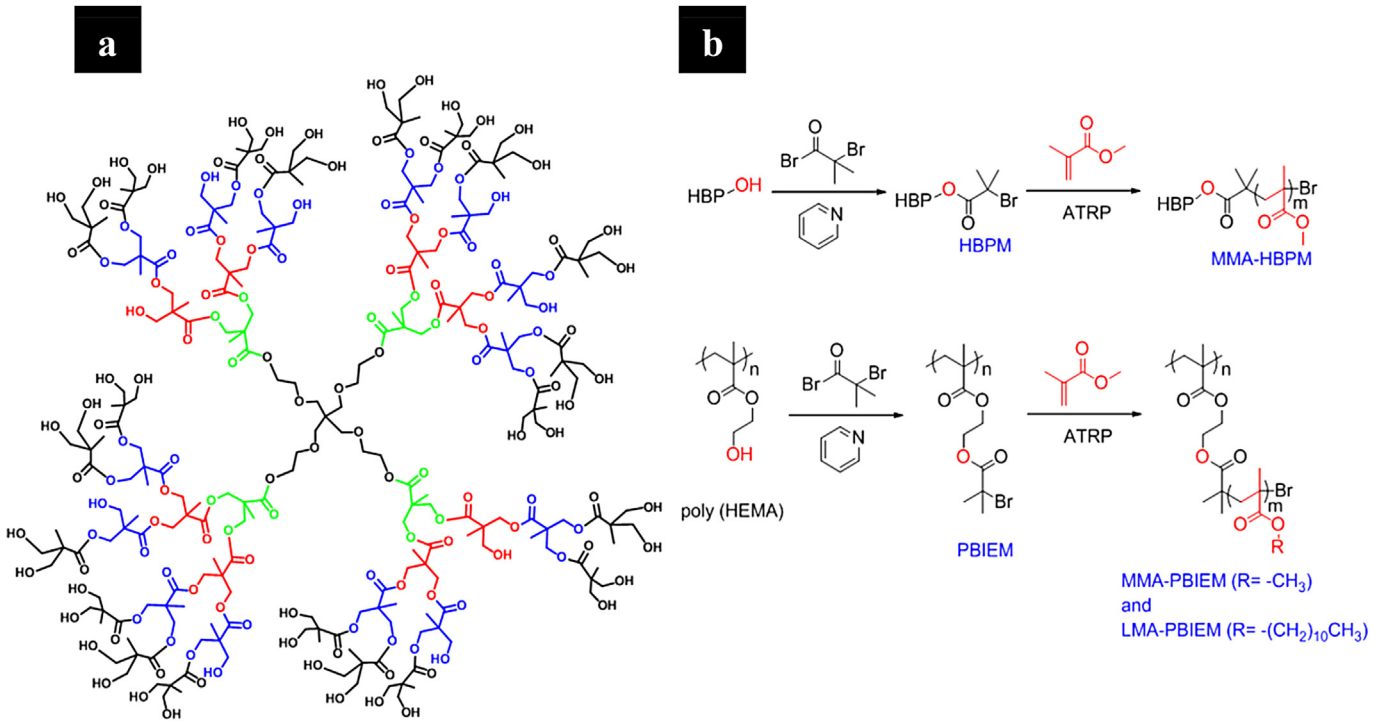

Scheme 1. (a) Chemical structure of hyperbranched bis-MPA polyester-64-hydroxyl, generation 4 (HBP–OH) (non dendrimer); and (b) synthesis procedure of spherical (MMA-HBPM) and cylindrical (MMA-PBIEM and LMA-PBIEM) hyperbranched polymers.

(300 MHz, Chloroform-d_1): δ: 0.90–0.95 ppm (–CH_3, 3H); 1.25–1.45 ppm (–$(CH_2)_{10}$–, 20H); 1.60–1.70 ppm (–CH_3, 3H); 3.97 ppm (–OCH_2–, 2H). M_n = 740,500 g/mol, and PDI = 6.45 (SEC chromatogram in Supporting Information).

2.3 Characterization

2.3.1. Chemical characterization

ATR-FTIR. Attenuated total reflectance Fourier transform infrared (ATR-FTIR) spectra of the polymer film were recorded on a Varian 660 IR spectrometer between 4000 and 600 cm^{-1} with a resolution of 2 cm^{-1} and 256 accumulated scans. The films were prepared by the solvent casting method from a chloroform solution (10 wt%) and dried under vacuum conditions until constant weight was reached.

Nuclear Magnetic Resonance (NMR). H NMR spectra of polymers were recorded with a Bruker Spectrometer, 300 MHz, using chloroform-d_1 as solvent. The deuterated solvent was used as the lock and TMS as the internal standard. Polymers concentration were 6.0 wt % and temperature 40 °C.

Size Exclusion Chromatography (SEC). Average molecular weight and molecular weight distribution were determined by Size-Exclusion Chromatography (SEC) in a LKB-2249 instrument at 25 °C. A series of four μ-Styragel columns (105, 104, 103, 100 Å pore size) were used with chloroform as eluent (good solvent for our systems and this solvent allows detection of carbonyl group by infrared analysis). Polymers concentration were 4–5 mg/ml, and flow rate was 0.5 ml/min (best resolution). The polymer was analyzed using infrared (IR) absorption at 5.75 μm with a Miram IA spectrophotometer detector. Methyl methacrylate standards supplied by Polymer Laboratories and Polysciences Inc. were used for calibration.

2.3.2. Thermal characterization

Thermogravimetric analysis (TGA). The polymers were characterized by thermogravimetric analysis (TGA) in TGA Q500-TA Instruments; and the equipment was kept under nitrogen atmosphere from room temperature to 900 °C, and gas purge was at 90 ml/min.

Differential Scanning Calorimetry (DSC). The thermodynamic properties of all the examined polymers were obtained from Mettler-Toledo DSC 1 STARe apparatus. The measuring device was equipped with a liquid nitrogen cooling accessory and a HSS8 ceramic sensor with 120 thermocouples. The samples were measured in an aluminum crucible (40 μL). During the standard measurement, temperature was increased at a heating rate equal to 10 K/min.

Temperature Modulated Differential Scanning Calorimetry (TMDSC). The frequency dependence of the calorimetric glass transition temperature was measured using a stochastic temperature-modulated differential scanning calorimetry (TOPEM) method implemented by Mettler Toledo DSC 1 STARe System. In these experiments, a slower heating rate equal to 0.5 K/min was applied. All measurements were conducted in a dry nitrogen atmosphere.

2.3.3. Broadband dielectric spectroscopy (BDS)

Isothermal, ambient pressure dielectric measurements at different temperatures were performed using a Novocontrol Alpha impedance analyzer at a frequency range of 0.1 Hz–10^6 Hz.Temperature was controlled using a Novocontrol Quatro Cryosystem with stability better than 0.1 K. Samples were placed in a parallel-plate capacitor of 15 mm diameter and with 0.1 mm glass fibers used as spacers.

3. Results and discussion

3.1. Polymer synthesis and characterization

ATPR polymerization produced hyperbranched polymers whose structure was confirmed by ATR-FTIR (cm^{-1}) and H NMR. Fig. 1

exhibits the FT-IR and H NMR spectra of the hyperbranched polymers obtained.

The IR spectra of spherical and cylindrical hyperbranched polymers (Fig. 1a and b) exhibited the typical functional group signals at the same wavenumber with different intensities: 2859–3000 (alkyl signals), 1730 (C=O), 1460 (C–H), 1390 and 1370 (C–H), 1270 (C–H α-Br), 1148 (C–O), 1100 (C–O α-Br), 1000–700 (irrelevant signals) 640 (C–Br). The absence of signals around 3000-3500 cm^{-1} suggest a complete reaction of bromoisobutyrate with the OH group of pre-polymers HBP-OH and Poly HEMA.

Fig. 1c and d shows the H NMR spectra of the hyperbranched polymers obtained; cylindrical hyperbranched polymers only displayed the signals of monomers (Fig. 1c) MMA and LMA, while both signals were observed in the MMA-HBPM spectrum, MMA monomer, and HBPM macroinitiator (Fig. 1d). This observation is explained by the high monomer concentration with respect to the macroinitiator PBIEM in MMA-PBIEM and LMA-PBIEM polymers, in line with the values of number-average molecular weight 25,700 g/mol for PBIEM, 500,000 g/mol for MMA-PBIEM and 740,500 g/mol for LMA-PBIEM. Regarding the spherical hyperbranched polymer, a different situation was noticed. Both signals were observed in the MMA-HBPM spectrum, since monomer concentration was comparable to the concentration of the spherical macroinitiator, also, in agreement with the values of number-average molecular weight 2050 g/mol and 11,000 g/mol for HBPM and MMA-HBPM, respectively.

Table 1
Isotactic (mm), atactic (mr) and syndiotactic (rr) percentages corresponding to peaks at 0.9 ppm, 1.07 ppm and 1.2 ppm, respectively.

Structure	% Isotactic (mm)	% atactic (mr)	% Syndiotactic (rr)
MMA-PBIEM	3.2	39.2	56.9
MMA-HBPM	11.5	40.3	48.2
Linear PMMA	4,3	39.0	56.7

The triad analysis of α-methyl signals of MMA-PBIEM (box in Fig. 1c) and MMA-HBPM (box in Fig. 1d) yielded different relative integration resulting from a change in tacticity due to the hyperbranched polymer morphology. Table 1 lists the isotactic (mm), atactic (mr) and syndiotactic (rr) percentages at peaks close to 0.9 ppm, 1.07 ppm and 1.2 ppm, respectively, for MMA-PBIEM, MMA-HBPM and a commercial non-hyperbranched PMMA (specifications in Materials section).

While the atactic percentage remained the same for all morphologies, MMA-HBPM yielded a higher isotactic percentage than MMA-PBIEM and PMMA (non-hyperbranched) did, suggesting a

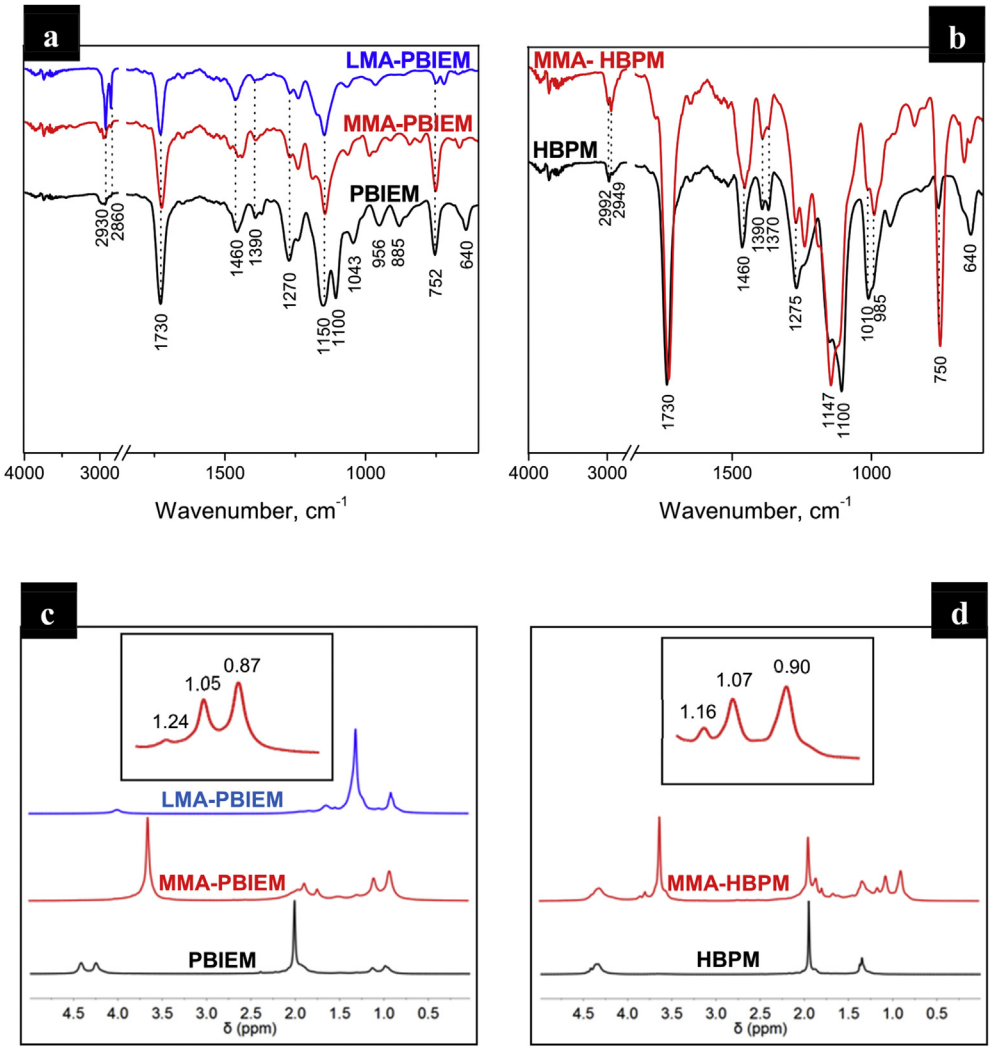

Fig. 1. FT-IR and H NMR spectra of hyperbranched polymers. a) and b) correspond to FT-IR of cylindrical and spherical hyperbranched polymers, respectively. c) and d) correspond to H NMR of cylindrical and spherical hyperbranched polymers, respectively.

specific stereochemistry as a function of the macroinitiator morphology. The spherical morphology allowed to obtain brushes with higher percentage of isotacticity. In turn, the cylindrical morphology presented brushes with a higher percentage of syndiotac ticity, similar to non-hyperbranched PMMA. The results suggest that this behavior could be ascribed to the 3D radial growth of the polymer chains. In fact, ATRP polymerization experiments with different initiator systems can produce molecular brushes with different stereochemistry.

3.2. Thermal properties

Thermogravimetric analysis allowed us to study the thermal stability of cylindrical and spherical polymers and to compare the properties of hyperbranched and non-hyperbranched PMMA polymers. Fig. 2 shows TGA curves, expressed in % weight in N_2 atmosphere for PBIEM, MMA-PBIEM and LMA-PBIEM (Fig. 2A), HBPM and MMA-HBPM (Fig. 2B), MMA-PBIEM, MMA-HBPM and non-hyperbranched PMMA (Fig. 2C).

Based on these results, the following order of stability can be established for the cylindrical hyperbranched polymers (Fig. 2a): LMA-PBIEM > MMA-PBIEM ≈ PBIEM. The thermal degradation of non-hyperbranched poly (n-alkyl methacrylates) such as PMMA and PLMA is essentially the reverse of its polymerization process, leading to monomer in 100% yield and PLMA has higher thermal stability [28,29]. In this particular case, LMA-PBIEM exhibited only one thermal event, probably due to the high monomer concentration with respect to the macroinitiator, while the presence of two thermal events for MMA-PBIEM could be attributed to different fragmentations of the polymer structures. For LMA-PBIEM, the initial degradation temperature (IDT) was higher than that of MMA-PBIEM, indicating that the introduction of the lauryl pendant group provides greater system stability. Conversely, the introduction of the methyl pendant group provided lower stability to the cylindrical hyperbranched system. Spherical MMA hyperbranched polymers displayed a similar stability behavior (Fig. 2b), two thermal events and similar stability between HBPM macroinitiator and MMA-HBPM.

If the decomposition profiles of macroinitiators PBIEM and HBPM are compared, both had two thermal events: PBIEM (with a molecular weight of repeat unit of 279 g/mol) lost 60% of its mass in the first thermal event, corresponding to the mass of α-bromoisobutyryl acid grafted into the Poly (HEMA). On the other hand, as demonstrated, the thermal properties of HBPM-based spherical hyperbranched polymers depend on the chemical structure of the end groups [30], as a consequence different types of interactions can occur and thermal stability may vary depending on the terminal group. In this case, HBPM (with a theoretical molar mass of 16,844 g/mol) lost 30% of its mass in the first thermal event, corresponding to the mass of 64 mol of HBr (64 OH esterified with α-bromoisobutyrate). These behaviors suggest different decomposition profiles for both macroinitiator systems. The percentages of mass loss in macroinitiators PBIEM and HBPM suggest a complete reaction of bromoisobutyrate with the OH group of pre-polymers HBP-OH and Poly HEMA. This is in agreement with the results of FT-IR, since the spectra did not show hydroxyl group signals.

Fig. 2c provides the stability order for methyl methacrylate polymers of different molecular architectures. As already mentioned, the thermal degradation of PMMA is essentially the reverse of its polymerization process, leading to a monomer in a 100% yield [31]. So much so that PMMA exhibited only one thermal event and initial degradation temperature (IDT) very similar to that of MMA-PBIEM and MMA-HBPM. Complex architectures seem to provide different fragmentations of the polymer structures. As a

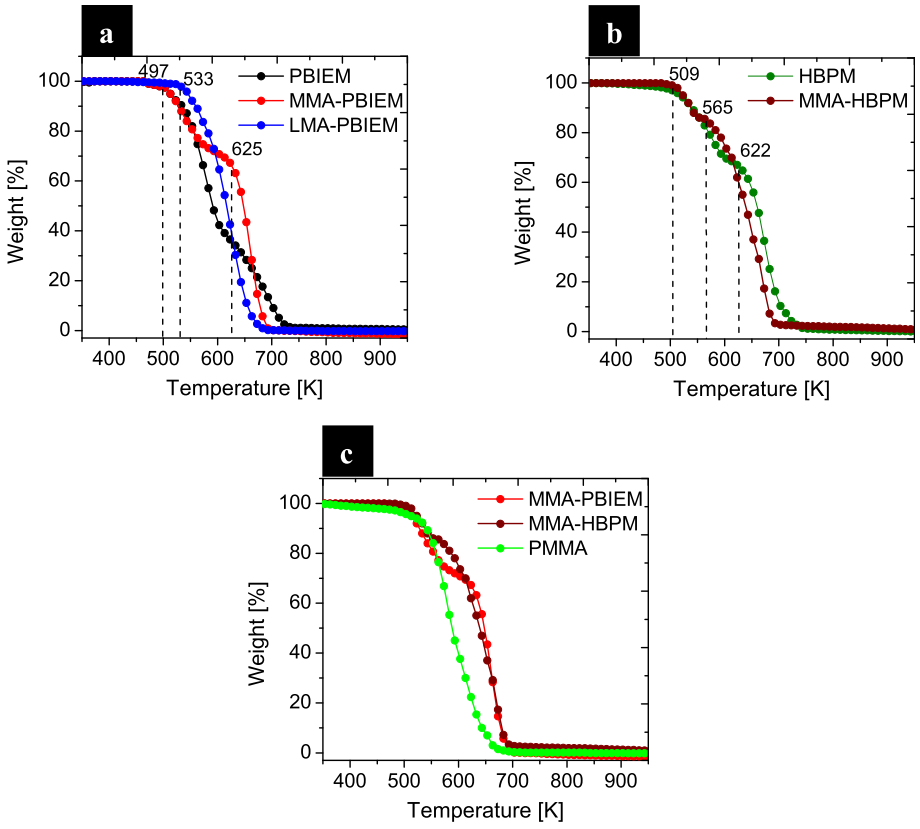

Fig. 2. TGA curves for (a) PBIEM, MMA-PBIEM and LMA-PBIEM (b) HBPM and MMA-HBPM and (c) MMA-PBIEM, MMA-HBPM and non-hyperbranched PMMA.

consequence, the hyperbranched PMMAs showed two thermal events, probably explained by the presence of the macroinitiator core and α-bromoisobutyryl end group, similar to block copolymers, also obtained by ATRP polymerization [32].

Differential scanning calorimetry (DSC) was the chosen method for monitoring the thermal transitions in the studied samples, which is very important to characterize new materials. DSC thermograms close to T_g values are shown in Fig. 3.

The observed glass transition region of the studied polymers showed important and interesting differences. Fig. 3a displays the thermograms of cylindrical hyperbranched polymers, PBIEM, MMA-PBIEM, LMA-PBIEM, and non-hyperbranched PMMA. Fig. 3b, in turn, shows the thermograms of spherical hyperbranched polymers, HBPM, MMA-HBPM and non-hyperbranched PMMA. In addition, Table 2 lists the glass transition temperature values of all the polymer structures. At first glance, the T_g value for the cylindrical hyperbranched polymers, MMA-PBIEM and LMA-PBIEM changed slightly with respect to the analogous non-hyperbranched PMMA and PLMA, respectively. In the case of MMA structures, the hyperbranched system yielded a T_g value 1.4 K higher than that of the non-hyperbranched system. With regards to the LMA systems, the hyperbranched structure yielded a T_g value 3.2 K lower than that of the non-hyperbranched system. A similar observation to that of the bottlebrush polymer T_g lying much closer to the T_g of the branch component was made by Grigoriadis [33] for bottlebrush $PBiBEM_{415}$-g-PBA.The fact that it is more visible in longer branches (PBA_{30}) is in agreement with our result. However, the T_g value of the spherical MMA structure showed an important difference: 45.7 K lower than that of the non-hyperbranched counterpart. This T_g value of MMA-HBPM indicates much less effective packaging of this structure due to the spherical architecture or shorter branches.

Based on TMDSC data for MMA, HBPM and MMA-HBPM, the composition of the hyperbranched polymer can be assessed. For this purpose, the Gordon–Taylor/Kelley-Bueche [34,35] equation is very often used for several materials such as copolymers and mixtures of both polymers and small molecular liquids. On the basis of this equation, we estimated that the weight fraction of PMMA was equal to 0.46.

With respect to macroinitiators, an interesting aspect is that the cylindrical structure PBIEM (T_g = 323.6 K) showed a T_g value lower than that of the pre-polymer Poly (HEMA) (T_g = 360 K) [37]; and the spherical structure HBPM (T_g = 297.9 K) showed a T_g value slightly higher than that of the pre-polymer HBP-OH (T_g = 295 K) [38] (see Scheme 1). The chemical modification of the OH groups by introducing a α-isobutyrate group changed the inter and intra-chain interactions. The absence of hydrogen bonds, led to a decrease in the glass transition temperature of the linear system PBIEM with respect to Poly HEMA. This effect is not observed in star systems. Additionally, the glass transition temperature of HBPM was slightly higher than that of the pre-polymer HBP-OH due to its spherical architecture.

Table 2
Glass transition temperatures obtained based on DSC (for a heating rate 10/min). *PLMA T_g value from Ref. [36].

Polymer	T_{gDSC} (K)
LMA-PBIEM	221.9
MMA-PBIEM	390.5
PBIEM	323.6
PMMA	389.1
HBPM	297.9
MMA-HBPM	343.4
PLMA	225.1*

3.3. Dielectric studies

Dielectric measurements were obtained in order to determine whether the structural findings above were reflected in the molecular dynamics of the synthetized materials of all the samples obtained. The representative spectra of hyperbranched polymers obtained by both macroinitiators are presented in Figs. 4–6. The temperature range and direction of the temperature change is labeled for each case in the panels. A common feature of the studied macroinitiators was their very complex dynamics. In both cases, a number of processes were visible both above and below the glass transition temperature (T_g).

As it can be noticed, above the glass transition temperature (T_g), almost all spectra exhibit a very strong dc-conductivity and electrode polarization effect. This is a typical situation for hyperbranched polymers that has been reported for other materials from this group as well [22,39]. Thus obtaining a straightforward determination of the segmental relaxation times (α) from the dielectric loss spectra (ε″) was impossible in almost all cases. However, it is well known that the same information about

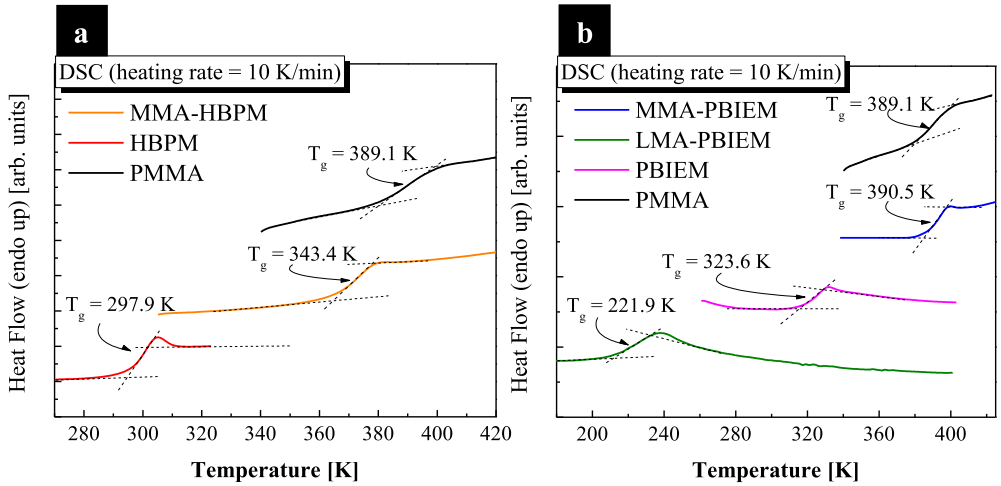

Fig. 3. Comparison of DSC thermograms of (a) MMA-PBIEM, LMA-PBIEM, PBIEM, PMMA and (b) MMA-HBPM, HBPM, PMMA. The PMMA and PLMA acronyms represent the non-hyperbranched PMMA and PLMA polymers.

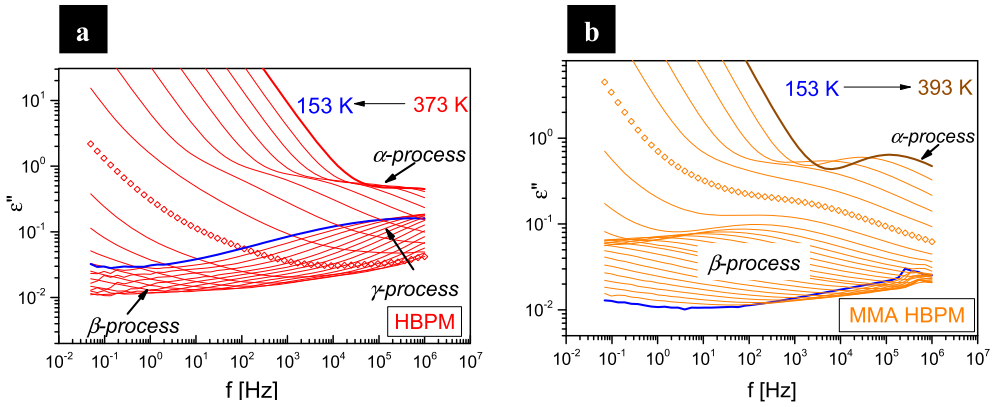

Fig. 4. Selected dielectric loss spectra of HBPM (a) and MMA-HBPM (b). The temperature range and direction of the experiment are labeled in the respective panels. The spectra marked with diamonds are taken almost at T_g. Panel (a) indicates the segmental and secondary relaxations.

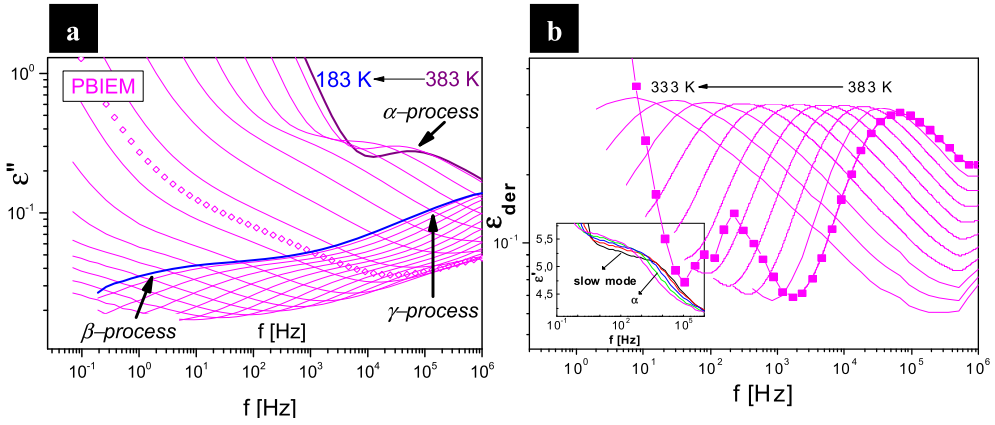

Fig. 5. (a) Selected dielectric loss spectra of PBIEM. The spectrum marked with diamonds is taken at a temperature very close to T_g. The horizontal arrow indicates the direction of the experiment. Temperature range is labeled. Clearly visible segmental and secondary processes are indicated with arrows (b) Examples of the spectra obtained as the derivative of ε' by means of equation (1) for PBIEM above T_g. For the highest temperature, also slow mode peak is presented. Inset: examples of the ε' spectra with clearly visible slow mode and segmental processes for PBIEM.

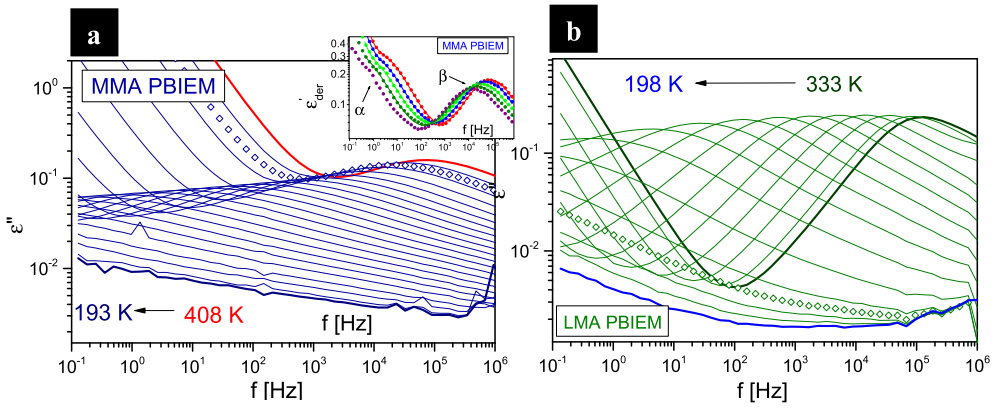

Fig. 6. Selected dielectric loss spectra of hyperbranched polymers MMA-PBIEM (a) and LMA-PBIEM (b). The temperature range and direction of the experiment are labeled in the respective panels. The spectra marked with diamonds are taken almost at T_g. Inset: examples of the ε_{der} spectra obtained from ε' by means of eq. (1) with segmental and secondary relaxation are indicated with arrows.

relaxation processes can be obtained from dielectric dispersion (see inset of Fig. 5b). In this case several methods can be applied, for instance, the analysis of ε' spectra or the transformation of dispersion (ε') into loss data (ε'') through the Kramers-Kronig relations or alternatively through logarithmic derivative [40].

$$\varepsilon_{der} = -\frac{\pi}{2}\frac{\partial\varepsilon'(\omega)}{\partial ln\omega} \quad (1)$$

In this study, the last method was applied. Its advantage is the presence of peaks with well-resolved maxima. This facilitates the

determination of relaxation times, which are estimated as the reciprocal of the angular frequency of the respective peak maximum. However, it should be borne in mind that, in such case, only the relaxation times can be analyzed since the shapes of the spectra obtained with eq. (1) differ from the experimental results [40]. The example of the ε″ spectra obtained from the transformed ε′ data can be seen in Fig. 5b. Along with segmental relaxation (α), slower relaxation process can be found above T_g (see inset of Fig. 5b). This process tends to merge the segmental relaxation in the vicinity of the glass transition. In our studies, this slow peak can be observed in both macroinitiators and in the MMA-HBPM sample.

Temperature dependence of relaxation times for the processes visible above T_g for HBPM and PBIEM based polymers are depicted in Fig. 7a and b, respectively. To compare the temperature dependence of the slow mode relaxation time of HBPM and its MMA polymer, the abscissa axis was rescaled by T_g (see inset of Fig. 7a). For both materials, the time scale of this movement is roughly the same. Interestingly, it seems to be slightly faster for the hyperbranched sample. For the two cylindrical macromolecules (MMA-PBIEM and LMA-PBIEM), the slow mode could not be observed. In the case of MMA-PBIEM, this could be ascribed to the fact that, in the temperature range of this experiment, the overall conductivity was so strong that it made very difficult to determine the segmental relaxation times (see inset of Fig. 6a). However, for LMA-PBIEM, the separation between dc-conductivity and the segmental relaxation peak was big enough to be sure that there was no such process present. As it can be seen in Fig. 6b, no additional peak can be seen in between. Thus, it can be speculated that also for MMA-PBIEM this type of motion becomes inactive.

Such slow modes can originate in various phenomena such as normal modes in polymers, interfacial polarization in heterogeneous materials, or changes in the H-bonded network. To study the behavior of ions in conductive materials, modulus representation ($M^* = 1/\varepsilon^*$) is often used [41–43]. By analyzing M″ spectra, the ionic relaxation times can be obtained. In the case of MMA-HBPM and HBPM samples, the relaxation times found in this way (half-filled diamonds) collapse almost perfectly into the data of the slow mode from the derivative representation shown in Fig. 7a. Thus, it can be concluded that the same ions are responsible for the ionic conductivity and the slow mode which is caused by ions movement in the interfacial voids (so-called Maxwell-Wagner-Sillars effect) [44]. Its absence in the cylindrical hyperbranched polymers and presence in the star hyperbranched polymer also give evidence of the fact that the branches in the bottlebrush polymer are much more densely packed. On the other hand, the similarity of the time scales of this movement in HBPM and MMA-HBPM indicates that the spatial heterogeneities in which this type of movement occurs are similar for both polymers. The segmental (α) relaxation times depicted in Fig. 6a and b (circles) were determined from the derivative of dispersion data (ε′) (eq. (1)). For both groups of materials, temperature dependence of the relaxation times was described with the Vogel - Fulcher -Tammann (VFT) equation:

$$\tau_\alpha(T) = \tau_\infty exp\left(\frac{DT_0}{T - T_0}\right) \quad (2)$$

where τ_∞ is the relaxation time at high temperature limit, D is the strength parameter, and T_0 is so-called Vogel temperature.

The dielectric glass transition temperature T_g obtained from these fits, together with the condition that $\tau_\alpha(T_g) = 100$s, correlates well with the calorimetric glass transition obtained via the DSC method. Based on the thermally modulated DSC measurements, segmental relaxation times could be determined in the vicinity of the glass transition temperature (represented in Fig. 7a and b with asterisks). The small discrepancies in PBIEM-based samples could again be attributed to the strong contribution of the low frequency processes, which prevents the exact determination of the dielectric α-relaxation times. Also, in some cases, it may be due to a large gap between the temperature ranges of the dielectric and the calorimetric experiments. In this case, the large uncertainty in the T_g cannot be avoided. This is caused by the long extrapolation of the VFT fits.

To compare how the different elements of the studied macromolecules influence their overall molecular dynamics, literature data of PMMA [45] (panel a), PMMA [34] and PLMA [36] (panel b) was added to the relaxation maps in Fig. 7. It is known that, in the case of PMMA, stereoregularity has a strong impact on the behavior of both segmental α-relaxation and secondary β-relaxation [19,45]. This is why, for comparison purposes with MMA-HBPM, the relaxation data from Shindo et al. (sample 5 in ref. 45) was used, which has tacticity closest to our sample (13% i, 33% h, 54% s). Certainly, in this comparison, the influence of the molecular mass on the dynamical properties, such as glass transition and fragility were not taken into account. Although, it is known that for high

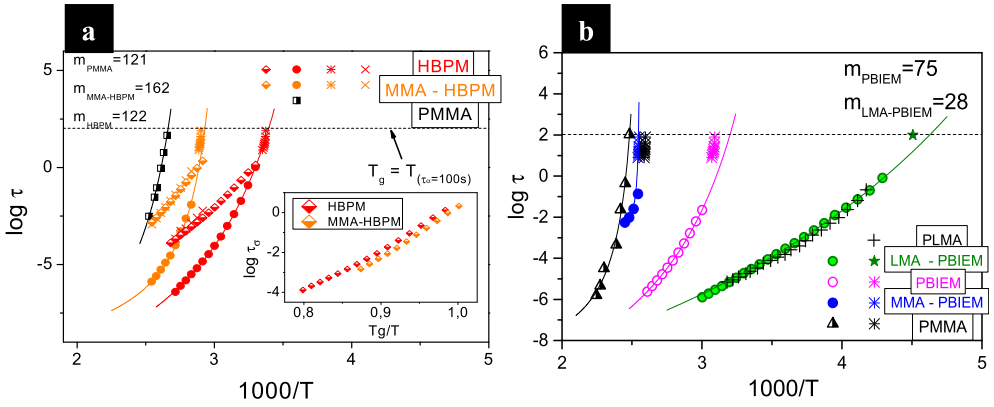

Fig. 7. (a)Temperature dependence of relaxation times of processes visible above T_g for HBPM (red points), MMA-HBPM (orange points) and PMMA (half-filled black squares) obtained by BDS (circles for α-process, crosses for slow-process, half-filled diamonds for ionic (σ) relaxation), TMDSC (asterisks). Data for the segmental mode of PMMA taken from reference [45]. Inset: comparison of temperature dependence of τ_σ for HBPM and MMA-HBPM vs. 1/T scaled by T_g. (b)Temperature dependence of segmental relaxation times for PBIEM (brown open circles –BDS, brown asterisks -TMDSC) and its hyperbranched analogues MMA-PBIEM (blue solid circles – BDS, blue asterisks - TMDSC) and LMA-PBIEM (green circles). For comparison, literature data for PLMA from ref. 36 (black crosses) and PMMA (half-filled black triangles from ref.46) are enclosed. Additionally TMDSC data of our linear PMMA are presented as black asterisks. For LMA-PBIEM, T_g from regular DSC experiment is presented as a green star. (For interpretation of the references to colour in this figure legend, the reader is referred to the web version of this article.)

molecular weight polymers the influence of molecular mass on the relaxation properties becomes negligible. This explains why we think that the data used provided a good qualitative idea of the relative positions of all the curves analyzed.

The analysis of the segmental α-relaxation in the studied hyperbranched polymers revealed a clear difference in the behavior of PBIEM- and HBPM-based macromolecules. As it can be observed, MMA-HBPM macromolecule behaves as expected on the basis of blends of low molecular compounds [47,48] or linear polymers [49]. Its glass transition temperature lies between values obtained from the components of our material. This means that the segmental dynamics is a combined effect of the two parts of the polymer (HBPM macroinitiator and PMMA branches). We also compared the so-called fragility or steepness index of the three samples. The values calculated for HBPM, PMMA and MMA-HBPM by means of the following relation:

$$m_P = \frac{d\log\tau_\alpha}{d(T_g/T)}\Big|_{T=T_g} \quad (3)$$

For $T_g = T$ ($\tau_\alpha = 100$s) are given in Fig. 7a. The fragility determined in this way represents the departure of temperature dependence of relaxation times from the Arrhenius behavior. In the case of the samples compared in Fig. 7a, it turned out to be much higher in the hyperbranched polymer than in both components. This means that temperature affects the mobility of the hyperbranched polymer more strongly than it does both building components.

A completely different behavior was found in PBIEM-based hyperbranched polymers. In this case, two different types of branches (PMMA or PLMA) were attached to the PBIEM macroinitiator. Temperature dependence of relaxation times obtained for the core and for both hyperbranched polymers is presented in Fig. 7b. Also, in this case, we found it interesting to compare how the molecular dynamics of the linear polymers, i.e., PMMA and PLMA, changed when they were anchored to the cylindrical core. The results are shown in Fig. 7b. As it can be seen, data sets for PLMA (taken from ref. [36]) and LMA-PBIEM collapse into one curve. This means that, in this case, the macroinitiator dynamics is completely suppressed and has no influence on the behavior (T_g or fragility) of the whole hyperbranched polymer. This situation is completely opposite to what was observed for MMA-HBPM. Thus, it should be determined whether this is caused by the long lauryl-side chain. For this reason, the data of MMA-PBIEM was also compared to that of PMMA. Indeed, the PMMA data used for comparison purposes in Fig. 7a has a slightly higher content of isotactic component if compared to MMA-PBIEM. As it has already been mentioned, this is important because the isotactic parts of PMMA reduce the glass transition temperature and fragility. Therefore, Fig. 7b includes data by Bergman et al. [46] with 85% of syndiotactic PMMA. Despite the fact that, at a first glance, it seems to be an exceedingly syndiotactic-rich sample, its T_g fits satisfactorily the one determined for our sample. Thus, it provides a quite good view on the position of the segmental relaxation times of PMMA with our tacticity. Moreover, the calorimetric relaxation times were determined on the basis of TMDSC experiments for the linear PMMA with the same tacticity as in our MMA-PBIEM. They are depicted in Fig. 7b as black asterisks. As it can be seen, they are well in line with the α-relaxation times of MMA-PBIEM. As stated above, the determination of the exact values of the segmental relaxation times for the MMA-PBIEM from the dielectric studies was problematic. In the inset of Fig. 6a, even in the derivative data obtained from eq. (1b), the low frequency side of the peak is not visible and the influence of the electrode polarization is so strong that the values obtained should be treated as a rough estimate. However, based on the experimental dielectric and calorimetric results as well as on literature data collected in Fig. 7b, it can be concluded that also in this case the dynamics of PBIEM does not influence the behavior of the studied hyperbranched macromolecule. This is congruent with the observation that no signal from PBIEM is visible in the H NMR of a PBIEM based hyperbranched polymer.

There is another interesting observation of the secondary or sub-T_g dynamics, which should be visible in the spectra collected in Figs. 4–6. Both macroinitiators below T_g have several active relaxation processes (see Figs. 4a and 5a), which is very common in polymeric materials [41,42]. For example, for PBIEM two processes faster than α relaxation are visible. However, when the spectra of both hyperbranched polymers with PMMA brushes are observed, only one process faster than the α-relaxation can be found. The relaxation times of this process for MMA-HBPM and MMA-PBIEM are collected and presented in Fig. 8. As it can be seen, for temperatures below T_g, the temperature dependence of relaxation times of this process follows the Arrhenius law given by the following equation:

$$\tau_\beta = \tau_\infty exp\left(\frac{\Delta E_\beta}{RT}\right) \quad (4)$$

where ΔE is an activation energy of the β-process. However, for MMA-PBIEM, a change of this dependence in the vicinity of the glass transition temperature can be observed. Above this temperature, it becomes steeper and no longer of Arrhenius type. Such scenario is, once again, well known from the data of the syndiotactic-rich PMMA samples. That is why the temperature dependence of the β-relaxation times below T_g of our hyperbranched polymer were compared to the results from ref. 46 (black crosses in Fig. 8). From a close inspection of Fig. 8, two observations can be made. First, for both studied materials, the relaxation times have almost the exact same values for the given temperatures. Certainly, this means that the activation energy determined by equation (4) is almost the same. The second observation is that there is only a slight difference between the secondary relaxation times of our dendrimers and the linear polymer from reference

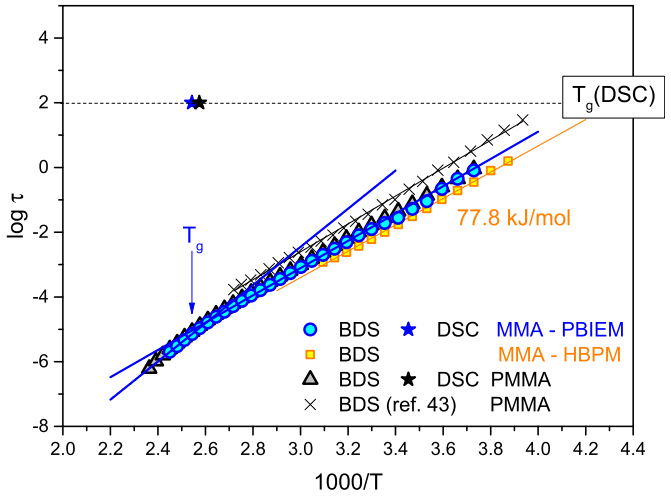

Fig. 8. Secondary relaxation times vs. 1000/T for MMA-PBIEM (blue circles) MMA-HBPM (purple squares) and for linear PMMA (grey triangles). For comparison purposes, β-relaxation times for temperatures below T_g from reference [46] (black crosses) are added. Black and blue stars indicate calorimetric T_g for linear PMMA and MMA-PBIEM, respectively, from regular DSC experiment. (For interpretation of the references to colour in this figure legend, the reader is referred to the web version of this article.)

[46]. The authors of this paper reported the value of activation energy as 18.96 kcal/mol or 79.5 kJ/mol. This value is very similar to our value of 77.8 kJ/mol. The activation of the β-process is very sensitive to the tacticity of PMMA, and it decreases as the amount of the isotactic component increases [45]. This supports our conclusion about the similarity between the materials studied by Bergman and by us. This also means that it is reasonable to take their data as reference. In fact, both of these observations indicate that the local dynamics of PMMA in the studied hyperbranched polymers is like that of the linear PMMA. Even the characteristic change of temperature dependence of the β-relaxation times in the vicinity of T_g (marked as a blue star in Fig. 8) is similar to the one observed in our MMA-PBIEM sample (see Fig. 2 in reference [46]). On the other hand, the local processes of the macroinitiators are completely suppressed, which means that both cores of the hyperbranched systems lose their internal chain mobility.

4. Conclusions

Based on the two macroinitiators with different structures (spherical and cylindrical), several hyperbranched polymers with tunable morphology and density of molecular brushes were obtained. Dynamic studies by broadband dielectric spectroscopy and stochastic temperature modulated DSC measurements revealed different patterns of behavior of hyperbranched polymers with different architectures. The behavior of the macromolecular system based on the spherical macroinitiator was similar to what is known from low-molecular blends or linear copolymers. Its segmental relaxation times (and T_g) were located between the relaxation times of both components while secondary relaxation came from PMMA, modified only by the change of the glass transition temperature. The unusual fact was that the local dynamics of HBPM core was not observed in the dielectric spectra of the hyperbranched molecule, which suggests that this macroinitiator became more rigid in the synthesized hyperbranched molecule. The other striking feature of this macromolecule is its extremely high fragility, which is much higher than that of both components. This result is probably related to the complex structure and bulkiness of this star polymer.

Cylindrical hyperbranched molecules behaved in a completely different manner. In the studied cases (MMA-PBIEM and LMA-PBIEM), the dynamics of the macroinitiator was completely suppressed, and that of the hyperbranched macromolecule was in fact the pure dynamics of its brushes. It is also worth mentioning that the packing of these brushes must be similar to that of their linear polymer counterparts, since the temperature dependence of relaxation times of LMA-PBIEM and PLMA overlap almost perfectly. Similarly, the only secondary relaxation found came from PMMA. It had exactly the same temperature dependence as MMA-HBPM did. Also the characteristic change of this dependence at the glass transition temperature is present. On the other hand, in the temperature range of the performed experiments, the β-process for LMA-PBIEM was not observed. However, it could have been hidden by the strong overlap of the segmental and secondary peaks. The question of whether this type of behavior is related to the cylindrical shape of its macroinitiator, dense packing or to the very high molecular weight of our bottlebrush hyperbranched macromolecules remains open as of today. Indeed further research should be conducted for a better understanding of this topic.

Acknowledgments

M. P. and Z.W. are deeply grateful for the financial support from the National Science Centre within the framework of the Maestro2 project (Grant No. DEC-2012/04/A/ST3/00337). We thank K. L. Ngai for helpful comments on the manuscript.

J.M.G and O.A. acknowledge financial support from CONICET, ANPCyT (PICT-2010-2554, PICT-2013-0905), Fundación Petruzza and the Austrian Institute of Technology GmbH (AIT–CONICET Partner Group: *"Exploratory Research for Advanced Technologies in Supramolecular Materials Science"* – Exp. 4947/11, Res. No. 3911, 28-12-2011). J.M.G. and O.A. are staff members of CONICET.

Appendix A. Supplementary data

Supplementary data related to this article can be found at http://dx.doi.org/10.1016/j.polymer.2016.08.027.

References

[1] B. Voit, J. Polym. Sci. Part A Polym. Chem. 38 (14) (2000) 2505–2525.
[2] B.I. Voit, A. Lederer, Chem. Rev. 109 (11) (2009) 5924–5973.
[3] L. Mei, Y. Jiang, S.-S. Feng, Nanomedicine 9 (1) (2014) 9–12.
[4] D.E. Poree, M.D. Giles, L.B. Lawson, J. He, S.M. Grayson, Biomacromolecules 12 (4) (2011) 898–906.
[5] Y. Zhou, W. Huang, J. Liu, X. Zhu, D. Yan, Adv. Mat. 22 (41) (2010) 4567–4590.
[6] U. Schlotterbeck, C. Aymonier, R. Thomann, H. Hofmeister, M. Tromp, W. Richtering, S. Mecking, Adv. Funct. Mat. 14 (10) (2004) 999–1004.
[7] X. Huang, P. Jiang, Adv. Mat. 27 (3) (2015) 546–554.
[8] M. Lv, S. Li, J.J. Jasieniak, J. Hou, J. Zhu, Z. Tan, S.E. Watkins, Y. Li, X. Chen, Adv. Mat. 25 (47) (2013) 6889–6894.
[9] T. Higashihara, M. Ueda, Macromolecules 0 (2) (2015), 150225100915008.
[10] D. Greszta, K. Matyjaszewski, Polym. Prepr. Am. Chem. Soc. Div. Polym. Chem.) 37 (1996) 569–570.
[11] R. Barbey, L. Lavanant, D. Paripovic, N. Schüwer, C. Sugnaux, S. Tugulu, H.-A. Klok, Chem. Rev. 109 (11) (2009) 5437–5527.
[12] C.J. Hawker, Angew. Chem. Int. Ed. Engl. 34 (13/14) (1995) 1456–1459.
[13] R. Hourani, A. Kakkar, Macromol. Rapid Commun. 31 (11) (2010) 947–974.
[14] K. Matyjaszewski, P.J. Miller, J. Pyun, G. Kickelbick, S. Diamanti, Macromolecules 32 (20) (1999) 6526–6535.
[15] K. Matyjaszewski, Macromolecules 45 (10) (2012) 4015–4039.
[16] J.F. Lutz, D. Neugebauer, K. Matyjaszewski, J. Am. Chem. Soc. 125 (23) (2003) 6986–6993.
[17] T. Nakano, M. Mori, Y. Okamoto, Macromolecules 26 (1993) 867–868.
[18] N.A. Porter, T.R. Allen, R.A. Breyer, J. Am. Chem. Soc. 114 (20) (1992) 7676–7683.
[19] N.G. McCrum, B.E. Read, G. Williams, Anelastic and Dielectric Effects in Polymeric Solids, Wiley, New York, 1967.
[20] M. Paluch, M. Sekula, S. Maślanka, K. Mańczyk, W.W. Sułkowski, S.J. Rzoska, J. Ziolo, J. Chem. Phys. 120 (4) (2004).
[21] A. Huwe, D. Appelhans, J. Prigann, B.I. Voit, F. Kremer, Macromolecules 33 (10) (2000) 3762–3766.
[22] J. Mijović, S. Ristić, J. Kenny, Macromolecules 40 (14) (2007) 5212–5221.
[23] K. Androulaki, K. Chrissopoulou, D. Prevosto, M. Labardi, S.H. Anastasiadis, ACS Appl. Mat. Interfaces 7 (23) (2015) 12387–12398.
[24] K. Grzybowska, Z. Wojnarowska, A. Grzybowski, M. Paluch, J.M. Giussi, M.S. Cortizo, I. Blaszczyk-Lezak, C. Mijangos, Polym. Guildf. 55 (4) (2014) 1–8.
[25] K.L. Ngai, T.R. Gopalakrishnan, M. Beiner, Polym. Guildf. 47 (20) (2006) 7222–7230.
[26] G. Kreutzer, C. Ternat, T.Q. Nguyen, C.J.G. Plummer, J.A.E. Månson, V. Castelletto, I.W. Hamley, F. Sun, S.S. Sheiko, A. Herrmann, L. Ouali, H. Sommer, W. Fieber, M.I. Velazco, H.A. Klok, Macromolecules 39 (13) (2006) 4507–4516.
[27] C. Li, N. Gunari, K. Fischer, A. Janshoff, M. Schmidt, Angew. Chem. - Int. Ed. 43 (9) (2004) 1101–1104.
[28] I.K. Varma, M. Varma Nair, V. Kumar Karan, D. Varma, Thermochim. Acta 141 (1989) 189–201.
[29] M. Demetriou, T. Krasia-Christoforou, J. Polym. Sci. Part a-Polymer Chem. 46 (2008) 5442–5451.
[30] J. Vuković, D. Steinmeier, M.D. Lechner, S. Jovanović, B. Božić, Polym. Degrad. Stab. 91 (8) (2006) 1903–1908.
[31] S.L. LeVan, Concise Encylopedia Wood & Wood-Based Mat. (1989) 271–273.
[32] L. Martin-gomis, M. Fernandez-García, J.L. de la Fuente, E.L. Madruga, M.L. Cerrada, Macromol. Chem. Phys. 204 (2003) 2007–2016.
[33] C. Grigoriadis, A. Nese, K. Matyjaszewski, T. Pakula, H.J. Butt, G. Floudas, Macromol. Chem. Phys. 213 (13) (2012) 1311–1320.
[34] J. Knapik, Z. Wojnarowska, K. Grzybowska, K. Jurkiewicz, L. Tajber, M. Paluch, Mol. Pharm. 12 (10) (2015) 3610–3619.
[35] W. Brostow, R. Chiu, I.M. Kalogeras, A. Vassilikou-Dova, Mat. Lett. 62 (17–18) (2008) 3152–3155.
[36] G. Floudas, P. Placke, P. Stepanek, W. Brown, G. Fytas, K.L. Ngai, Macromolecules 28 (20) (1995) 6799–6807.
[37] T. Caykara, C. Özyürek, Ö. Kantoglu, J. Appl. Polym. Sci. 103 (2007) 1602–1607.
[38] M. Rogunova, T.Y.S. Lynch, W. Pretzer, M. Kulzick, A. Hiltner, E. Baer, J. Appl. Polym. Sci. 77 (2000) 1207–1217.

[39] J.R. Sangoro, G. Turky, M.A. Rehim, C. Iacob, S. Naumov, A. Ghoneim, J. Kärger, F. Kremer, Macromolecules 42 (5) (2009) 1648–1651.
[40] M. Wübbenhorst, J. van Turnhout, J. Non. Cryst. Solids 305 (1–3) (2002) 40–49.
[41] K. Androulaki, K. Chrissopoulou, D. Prevosto, M. Labardi, S.H. Anastasiadis, ACS Appl. Mat. Interfaces 7 (23) (2015) 12387–12398.
[42] P.W. Zhu, S. Zheng, G. Simon, Macromol. Chem. Phys. 202 (15) (2001) 3008–3017.
[43] K. Adrjanowicz, K. Kaminski, M. Dulski, M. Jasiurkowska-Delaporte, K. Kolodziejczyk, M. Jarek, G. Bartkowiak, L. Hawelek, S. Jurga, M. Paluch, Macromolecules 47 (16) (2014) 5798–5807.
[44] H. Lu, X. Zhang, H. Zhang, J. Appl. Phys. 100 (5) (2006).
[45] H. Shindo, I. Murakami, H. Yamamura, J. Polym. Sci. Part A-1 Polym. Chem. 7 (1) (1969) 297–310.
[46] R. Bergman, F. Alvarez, A. Alegrıa, J. Colmenero, J. Non. Cryst. Solids 235–237 (1998) 580–583.
[47] K. Kaminski, E. Kaminska, E. Chelmecka, M. Paluch, J. Ziolo, P. Wlodarczyk, K.L. Ngai, J. Phys. Chem. B 112 (2008) 7662–7668.
[48] T. Blochowicz, E.A. Rössler, Phys. Rev. Lett. 92 (22) (2004), 225701-1.
[49] A. Bartolotta, G. Carini, G. D'Angelo, G. Di Marco, Y. Gorodilov, E.G. Privalko, V.P. Privalko, B.N.A. Rekhteta, G. Tripodo, J. Phys. Condens. Mater 15 (11) (2003) S987.